Admittance studies of surface quantization in [100]-oriented Si metal-oxide-semiconductor field-effect transistors*

A. M. Voshchenkov† and J. N. Zemel
University of Pennsylvania, Philadelphia, Pennsylvania 19174
(Received 12 March 1973)

The behavior of charge carriers in the inversion layer under surface-quantized conditions was observed by small-signal magnetoadmittance (Y) and manetoconductance (G) experiments on p-type (100) Si metal-oxide-semiconductor field-effect-transistor (MOSFET) structures. The two-dimensional character of the surface-quantized electron gas was further substantiated. The density of states was studied directly by the surface-capacitance technique. The dependence of Y on a number of variables was investigated, including (1) $T \leq 4.22\,^{\circ}$K, (2) magnetic field ($B \leq 12$ T), (3) electric field excitation, (4) frequency, and (5) substrate doping ($10^{19} \leq p \leq 2\times10^{20}/\mathrm{m}^3$). Comparative studies of small-signal surface conductance and admittance were useful in establishing the advantages and limitations of each technique. It was observed that Y becomes frequency independent at frequencies below 500 Hz. Both the line shape and fine structure observed at Y at threshold are attributed to a bound-state band overlapping the conduction band resulting from surface-potential fluctuation. Circuit modeling of the MOSFET structures was found to be important in the interpretation of the admittance.

I. INTRODUCTION

Surface quantization is the term applied to the formation of a two-dimensional electron gas (2DEG) at the surface of a semiconductor. This 2DEG is a result of the large electric field associated with a strongly inverted or accumulated surface area. Thus, the space charge is quantized in the normal (z) direction, although there is no restriction in the plane of the surface. The elucidation of phenomena associated with surface quantization (SQ), and the expansion of techniques available to the experimentalist in this area, have been the motivation for the present study.

With the successful development of the metal-oxide-semiconductor (MOS) structure it became possible to test Schrieffer's proposal[1] that, under strong band-bending conditions, bound states for motion perpendicular to the surface in the bulk direction may exist. In 1966, low-temperature magneto-oscillatory conductance measurements of the Schubnikov–de Haas type revealed that the electronic density of states in a deeply inverted (100) silicon surface was two-dimensional, implying quantization of motion in the z direction.[2] In 1968, the small-signal surface capacitance was used to investigate SQ.[3,4] Performing magnetocapacitance experiments, it was possible to confirm the two-dimensional nature of the surface electron gas. In addition, it was observed that the capacitance threshold (turn-on) occurred at lower gate voltages than conductance, thereby enabling the study of a portion of the density of states which could not be observed by magnetoconductance experiments. In 1967, Duke[5,6] began theoretical studies of SQ in the accumulation region. He constructed a self-consistent model for the shallow band bending of an electron-accumulation region. From the binding energies and wave functions for the normal-motion bound states, he derived expressions for the contribution to the absorption coefficient due to vertical transitions among the two-dimensional electric subbands. This, in part, motivated Ralston[7] and Ralston and Wheeler[8] to attempt subband-absorption experiments. In 1971, they reported the observation of a channel-admittance modulation attributed to optical transitions on the (100) surface of silicon. The photoadmittance response due to a 44.3-meV (27.97 μm) photon was a negative, smeared, line spectrum suggesting the existence of several (5) electron subbands. It was proposed that the drastic reduction of electron mobility in the excited quantized states caused the negative photoadmittance observed.

The self-consistent calculations of Stern and co-workers[9–11] have yielded considerable information on the inversion layer. Ohta[12,13] has carried out a series of calculations on the effect of broadening of the Landau levels of a two-dimensional electron gas on both surface capacitance and conductance. Ohta employed a Green's-function propagator method to explore single and multiple scattering from impurities. Roughness and phonon scattering of the 2DEG is neglected. Recent calculations by Ando[14] on inhomogeneities and by Matsumoto[15] on surface roughness indicate that these processes will influence the scattering lifetime of carriers in a 2DEG. Ezawa has also considered the influence of phonon scattering on the surface mobility when two-dimensional effects dominate transport behavior.[16] All of the theoretical efforts tend to emphasize scattering effects (with the exception of Ohta's paper on capacitance), reflecting the large amount of experimental data on surface

transport.

In this paper, the experimental determination of some properties of the 2DEG are presented. Small-signal magnetoadmittance studies of inversion layers on p-type (100)-oriented metal-oxide-semiconductor field-effect transistors (MOSFET's) are reported. The useful regimes of magnetoadmittance studies were established and a circuit model of the MOSFET capacitor was studied. Comparative studies of magnetoconductance and magnetoadmittance established the usefulness of both techniques, as well as their interdependence. The magnetoadmittance experiments were conducted as a function of magnetic field ($B \leq 12$ T), measuring electric field ($F \leq 4\times 10^4$ V/m), temperature ($T \leq 4.22$ K), frequency (160 Hz $\leq f \leq$ 90 kHz), and substrate resistivity ($1 \leq \rho \leq 50$ Ω m).

All experiments were performed in the small-signal regime. Therefore, in the continuing text, the words "small signal" will be omitted in most cases, but it is to be understood that the capacities and conductivities measured are small-signal or differential quantities. Therefore, $C = dQ/dV$ and $g = e\Delta n\mu$, where C is the small-signal capacitance, Q is the charge, V is the ac voltage, e is the charge of an electron, Δn is the differential number of carriers due to V, and μ is the mobility of the minority carriers.

Finally, a one-electron model for the 2DEG is employed to interpret the data. The simplicity of the one-electron model is more important than the possible errors caused by failure to account for interaction effects. A δ-function model for the Landau quantization proves adequate for explaining the turn-on behavior observed.

II. PHENOMENOLOGICAL THEORY

In three-dimensional $\vec{k}$ space, the Si-electron constant-energy surfaces are ellipsoids of revolution, the energy expression for each valley being

$$E = (\hbar^2/2)(k_l^2/m_l + k_t^2/m_t), \tag{2.1}$$

where the longitudinal (l) direction is the major axis of the ellipsoid, and the transverse (t) direction is the minor axis. The longitudinal mass for silicon is $m_l = 0.98m_0$, and the transverse mass is $m_t = 0.19m_0$, where m_0 is the free-electron mass.

In our experiments the surface was quantized by inducing an n-type surface charge on a p-type Si substrate. If the [001] direction (normal) is chosen as the direction of quantization, then two valleys contribute to the lowest-energy, [i.e., heavy-mass (m_l)] subband for conduction along the [001] direction. The other four light-mass (m_t) valleys contribute to the next higher subband (see Fig. 1).[9] Taking account of spin and valley degeneracy, g_s and g_v respectively, the density of states of the 2DEG is

$$N_{2D}(E) = \left(\frac{g_s g_v}{\hbar^2}\right)\frac{m^*}{2\pi} \text{ per unit area } (E \geq E_0), \tag{2.2}$$

where E_0 is bottom of the two-dimensional density of states (2DDS). It is seen that the 2DDS per unit area is energy independent and is dependent on the density-of-states effective mass.

As pointed out above, the induced electron charge forms the 2DEG. To obtain quantitative information, the experiment has to relate this induced charge to more fundamental parameters. At low temperatures and for reasonably thick oxides ($d_{ox} \gg d_{inv}$, where d_{ox} is the oxide thickness and d_{inv} is the inversion layer thickness), the total mobile inversion charge per unit area, $-Q_{inv}$, is defined in terms of the gate voltage V_G and the threshold voltage V_T as

$$-Q_{inv} = -C(V_G - V_T) = -en_{inv}, \tag{2.3}$$

where n_{inv} is the number of inversion charges and C is the total capacity.[18] The effect of oxide charge and metal-semiconductor work-function differences are included in V_T, the threshold voltage necessary for the formation of free charge carriers at the surface. In the electric quantum limit where only the lowest subband is occupied, n_{inv} can be written as

$$n_{inv} = \int_{E_0}^{\infty} N_{2D}(E) f(E)\, dE, \tag{2.4}$$

where $f(E)$ is the Fermi function. Since $N_{2D}(E)$ is energy independent, it can be removed from the integral, and Eq. (2.3) can be rewritten with the aid of Eq. (2.4) so that

$$V_G = V_T + (eg_s g_v m^*/2\pi\hbar^2) F_0((E_F - E_i)/kT), \tag{2.5}$$

where $F_0(x)$ is the Fermi integral of zero order, E_F is the Fermi energy and E_i is the intrinsic

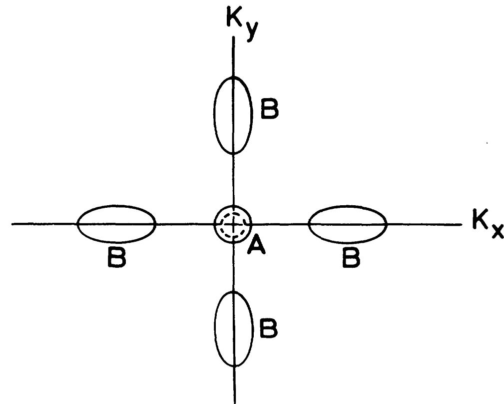

FIG. 1. (100)-oriented n-type silicon constant-energy surfaces. The (A) valleys are the doubly degenerate heavy-mass valleys produced by the surface potential while the (B) valleys are the fourfold degenerate light-mass valleys.

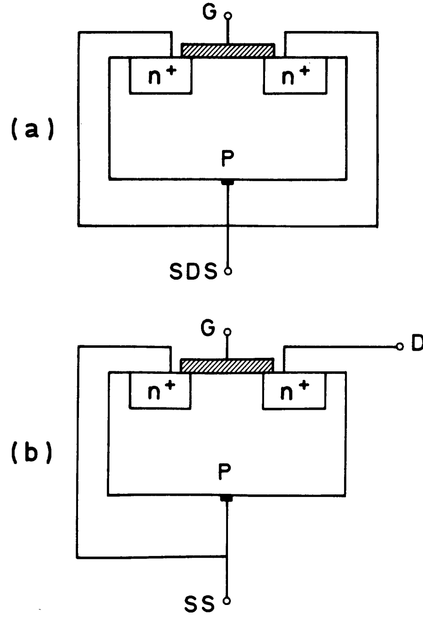

FIG. 2. MOSFET configuration for (a) capacitance and (b) conductance experiments.

Fermi energy. The 2DEG can be further quantized by imposing a magnetic field with a component perpendicular to the silicon surface. The existing electric-field-induced subbands are further split into an interlacing ladder of Landau levels separated by the cyclotron energy $\hbar\omega_c$ starting from each subband. The energy eigenvalues including spin and valley splitting are[9]

$$E' = E_0 + (n+\tfrac{1}{2})\hbar\omega_c + sg\mu_B B_z + vE_v(B_z), \qquad (2.6)$$

where $s=\pm\frac{1}{2}$ (spin quantum number), g is the Landé g factor,[17] $v=\pm\frac{1}{2}$ (valley quantum number), and $E_v(B_z)$ is the energy of the valley split level. The origin of the magnetic field dependence of E_v is not known at this time. Since there must be total state conservation, each Landau level must have $\hbar\omega_c N_{2D}(E)$ states. Each successive filled Landau level should have exactly the same amount of charge as the previous one.

III. EXPERIMENTAL CONSIDERATION

A. MOSFET capacitor

The experimental configuration for a MOSFET capacitor is shown in Fig. 2(a). The source is shorted to the drain. This is then connected to the substrate of the MOSFET. The capacitance is measured with respect to the gate electrode.

In Fig. 3, the lumped equivalent circuit for the shorted source-drain-to-gate capacitor is shown. In fact, the MOSFET is a distributed element, but the difficulties in handling the distributed MOSFET equivalent circuit are substantial. The lumped-circuit model provides a general qualitative picture of the behavior of both the real and imaginary parts of the admittance. Any attempt to draw quantitative conclusions from the lumped model would be inappropriate because of the large errors that arise. It is simple to show that the admittance for the lumped model is

$$Y = \frac{j\omega C_{ox}[1+\omega^2 R'^2 C'(C'+C_{ox})]}{1+\omega^2 R'^2 (C'+C_{ox})^2} + \frac{\omega^2 C_{ox}^2 R'}{1+\omega^2 R'^2 (C_{ox}+C')^2}, \qquad (3.1a)$$

$$\frac{1}{R'} = \frac{R_{inv} C_{inv}^2 \omega^2}{1+\omega^2 R_{inv}^2 C_{inv}^2} + \frac{R_{dep} C_{dep}^2 \omega^2}{1+\omega^2 R_{dep}^2 C_{dep}^2}, \qquad (3.1b)$$

$$C' = \frac{C_{inv}}{1+\omega^2 R_{inv}^2 C_{inv}^2} + \frac{C_{dep}}{1+\omega^2 R_{dep}^2 C_{dep}^2}, \qquad (3.1c)$$

where C_{ox} is the oxide capacitance, and the inv and dep subscripts indicate parameters which are associated with the inversion and depletion regions, respectively. The capacitance of the system for a sinusoidal excitation is then defined as

$$C = (\mathrm{Im}\,Y)/j\omega \qquad (3.2)$$

and the parallel conductance is

$$G_p = \mathrm{Re}\,Y. \qquad (3.3)$$

For convenience, the magnitudes of C and G_p in between Landau levels and at the peak in the Landau level are shown in Table I. At turn-on, the values of C and G_p should roughly correspond to their values in between Landau levels. When the device is fully turned off, G_p will be essentially zero and $R' \sim \infty$. From there G_p rises to a peak of 10^{-9} mho as the Fermi level moves into the 2DDS. In between Landau levels, or near turn-off, G_p drops to a maximum value of 10^{-12} mho. Peaks in G_p will therefore occur at turn-on and in between Landau levels (see Fig. 17 for an example). The surface states are in parallel with the inversion-layer charge. At the temperatures where the measurements were conducted, the normally observed room-temperature surface states are essentially frozen out. Hence, only the inversion and depletion charge will be considered. The geometric

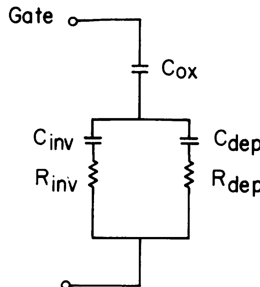

FIG. 3. Shorted source-drain-substrate.

TABLE I. Values for the total capacitance in between Landau levels (turn-off) and at the peak of the Landau levels (turn-on). R' and C' are estimated from experimental observations on devices used.

	Turn-off	Turn-on
	$R' \gg 10^3\ \Omega$	$R' \ll 10^3\ \Omega$
	$C' \ll C_{ox} \approx 10^{-11}$ F	$C' \gg C_{ox} \approx 10^{-11}$ F
	$\omega < 10^4$/sec	$\omega < 10^4$/sec
C	$C_{ox}C'/(C_{ox}+C') \approx C'$	$C_{ox}(1-\omega^2 R_1^2 C_{ox} C') \approx C_{ox}$
G_p	$1/R \approx 10^{-9}$ mho	$\omega^2 C_{ox}^2 R' \approx 10^{-12}$ mho

overlap capacity C_{ov} due to the overlap of the gate onto the source and drain diffusions (see Fig. 6) adds in parallel with C, and therefore the total capacitance C_T is

$$C_T = C_{ov} + C . \tag{3.4}$$

Notice that the description so far concerns only the circuit properties of a real MOSFET capacitor, and yields no insight into the physical properties of surface quantization. Surface quantization enters into the circuit model in the form of C_{inv}. Hence, the effects due to changes in C_{inv} should be separated analytically from variations in the circuit properties of the system. This obviously complicates the admittance study of surface quantization. Combining both the limitations due to the one-electron-model[9–14] surface quantization and the lumped-circuit picture prevents us from obtaining a detailed description of the surface-quantized MOSFET circuit.

B. Conductance measurements

The experimental connections of the devices for the conductance measurement is shown in Fig. 2(b). The channel conductance of a MOSFET, under the condition of zero source-drain dc voltage, is given by

$$G_{sd} = -(Z/L)\mu_n Q_{inv} , \tag{3.5}$$

where μ_n is the mobility of the electrons in the inversion region and Z/L is the ratio of the channel width to channel length. The small-signal conductance is

$$g_{sd} = -(Z/L)\mu_n \Delta Q_{inv} , \tag{3.6}$$

where ΔQ_{inv} is the inversion-layer charge which responds to the small-signal excitation. Care must be taken so that the period of excitation is greater than the transit time of the electrons from source to drain.

When transit-time effects can be neglected, $\Delta Q_{inv} = Q_{inv}$ and

$$g_{sd} = -(Z/L)\mu_n Q_{inv} . \tag{3.7}$$

It is obvious from Eq. (3.7) that only the product $\mu_n Q_{inv}$ can be obtained from conductance experiments. This is a fundamental limitation of conductance measurements. Only capacitance can be directly related to the density of states.[3]

IV. MEASUREMENTS

The measurements were fairly conventional with some exceptions. The Bitter magnet[19] produces substantial microphonic noise unless care is taken. The leads to the MOSFETs were all individually shielded by mounting them coaxially in $\frac{1}{8}$-in. nonmagnetic stainless-steel tubes. A polyvinyl spaghetti was used to provide spacing inside the tubing. Care was taken to avoid inductive loops throughout the whole insert. External electrical contacts allowed the device to be configured for either admittance or surface-conductance measurements. Thus, direct comparison of the two types of measurements could be easily accomplished.

A. Bridge admittance measurements

The block diagram of the measurement circuit is shown in Fig. 4. The basic technique consists of measuring an off-null voltage from the output of an admittance bridge. An external source is used to provide the ac voltage which is applied to the gate of the MOSFET capacitor through the bridge itself. The device capacitance C and effective parallel conductance G_p (loss term) can be nulled-out at some convenient point, such as deep inversion, and calibrated also at one point on the accumulation side. As the ramp sweep (dc gate-voltage supply) drives the surface from deep inversion towards accumulation, C' will change appreciably and both C and G_p will change, thereby unbalancing the bridge. The off-null voltage is measured by a modified PAR HR-8 phase-sensitive detector, which can measure the in-phase (G_p) signal and the out-of-phase signal (C) with high precision. In this manner, C vs V_G and G_P vs V_G can be recorded consecutively. It has been empirically determined

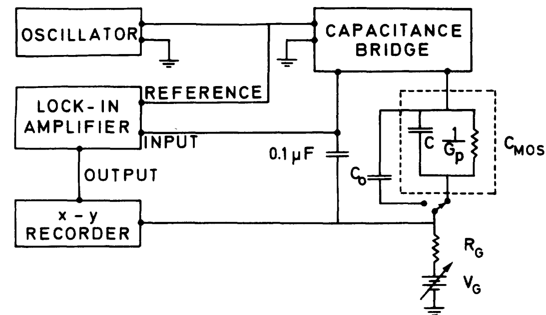

FIG. 4. Block diagram for the bridge-type small-signal surface-capacitance measuring technique.

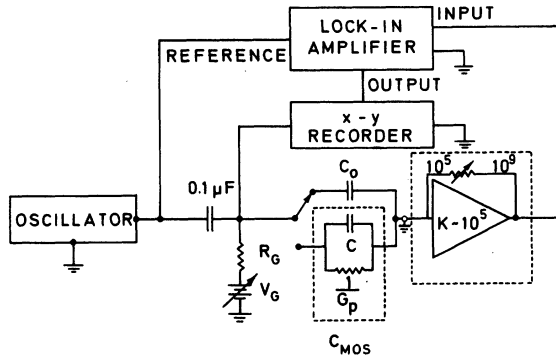

FIG. 5. Block diagram for the direct-type small-signal surface-capacitance measuring technique.

that the off-null voltage nonlinearity of the bridge is no more than 0.2% of full scale. Therefore, since two extreme points are calibrated, the variation between these points is known within 0.2%.

B. Direct admittance measurement

The block diagram for the direct admittance measurement is shown in Fig. 5. A constant ac excitation voltage is applied directly to the gate, and the output current of the device is then measured. The ratio is the admittance. The advantage of this method is that the signal is unaffected by coaxial-lead shunt capacitance, and yields a much better signal-to-noise ratio. In addition, since there is no internal bridge impedance, it is possible to use much lower frequencies. In fact, the only limitation is the internal impedance of the device itself at low frequencies, and the sensitivity and internal noise of the front end of the phase-sensitive detector.

C. Transformer-coupled measurement of small-signal conductance

The experimental procedures followed in the measurement of small-signal conductance are identical to those used by Fang, Fowler, Howard, and Stiles.[2]

V. DEVICE CHARACTERISTICS

The simplified device geometry is shown in Fig. 6. All MOSFETs had p-type boron-doped substrates with initial doping levels of 10^{19} m^{-3} (5–150 Ω m) $\leq N_A - N_D \leq 1.5\times10^{20}$ m^{-3} (1 Ω m). After processing, the initial substrate resistivities decreased to $1.40 \geq \rho \geq 0.70$ Ω m, due to thermal-conversion effects. The source-drain regions were phosphorous-doped to the maximum solubility level of phosphorus in silicon (i.e., $n \simeq 10^{26}$–10^{27} m^{-3}). A drive-in diffusion was used to achieve a junction depth of 1 μm.[18] The thermally grown SiO_2 was about 0.27 μm thick on most devices and had a relative dielectric constant of $\epsilon_{ox} = 3.85$. The channel length was 10 μm, and the channel width-to-length ratio was $Z/L \simeq 60$. A 1-μm aluminum metallization was used for the gate overlapping both the source and the drain (Fig. 6).

VI. DISCUSSION OF RESULTS

A. Room temperature

A typical room temperature C-V_G curve is shown in Fig. 7. Because of the n-type contacts at the surface, the device does not exhibit accumulation behavior. The net interface charge $Q_{int} = Q_{ss} + Q_{ox}$, consisting of surface-state and oxide charge, was evaluated in the following manner. The voltage associated with C_{min}, which occurs in the weak-inversion regime, was compared with an ideal value calculated from known values of d_{ox}, substrate doping $N_A - N_D$, and the metal-semiconductor work-function difference.[20] The net interface charge could then be determined by

$$\Delta V_{min} = V_{min}(\text{ideal}) - V_{min}(\text{observed}) = Q_{int}/C_{ox} . \tag{6.1}$$

Oxide breakdown was checked by subjecting all devices to $V_G = 40$ V.

B. Cryogenic temperature

At cryogenic temperatures, threshold is defined to correspond to the gate voltage at which the Fermi level lies within $3kT$ of the two-dimensional band edge. The justification for this definition lies in the fact that appreciable filling of a band does not occur until the Fermi level is within $3kT$ of the edge (the conventional definition of degeneracy). In this work we are concerned with metallic degeneracies in the 2DDS. Hence, the onset of transport in the 2DEG is associated with the onset of degeneracy. V_T can be generalized from the work of Heiman and Miller[21]:

$$V_T = -\frac{1}{C_{ox}}(Q_{int} + Q_{D,T}) + \varphi_{MS} + V_{D,T}, \tag{6.2}$$

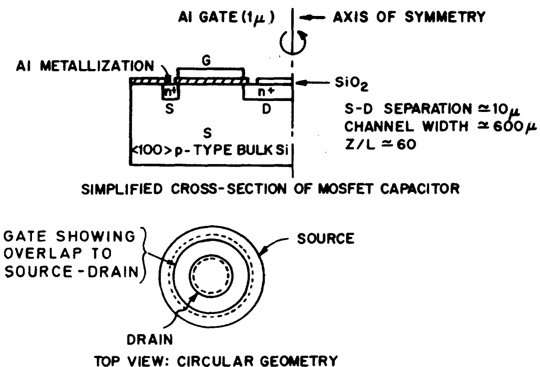

FIG. 6. Circular geometry MOSFET structure.

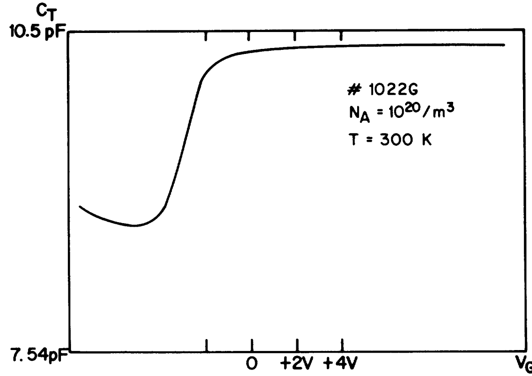

FIG. 7. Typical C-V curve at room temperature.

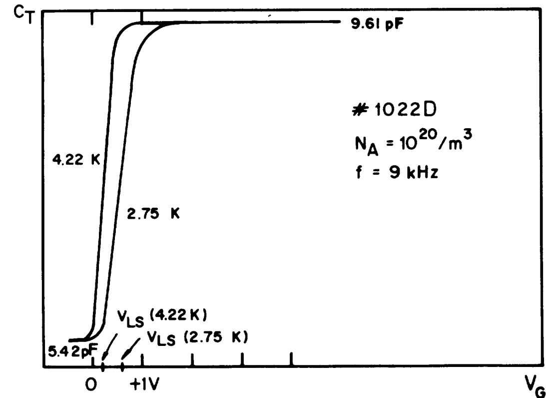

FIG. 8. Temperature dependence of C-V curve turn-on line shape.

where φ_{MS} is the metal-semiconductor work-function difference, $Q_{D,T}$ is the maximum depletion charge at threshold,

$$Q_{D,T} = -qN_A Z_d = -(2\epsilon_0\epsilon_{Si} qN_A V_{D,T})^{1/2}, \qquad (6.3)$$

$V_{D,T}$ is the voltage drop across the depletion region at threshold,

$$qV_{D,T} = (E_c - E_v) + (E_v + E_F) - 3kT$$
$$\simeq (E_g - 3kT) + kT\ln(N_A/A_P) \simeq E_g, \qquad (6.4)$$

and A_P is the effective valence-band density of states,[22]

$$A_P = 0.92(2\pi mkT/h^2)^{3/2}.$$

The quantity φ_{MS} is typically 1.1 V for the metals considered here, while $V_{D,T}$ is approximately equal to the band gap ϵ_g, and is 1.2 V. From the above values we observe that

$$-\varphi_{MS} \simeq V_{D,T}. \qquad (6.5)$$

Consequently, Eq. (6.2) reduces numerically to

$$V_T = (1/C_{ox})(Q_{int} + Q_{D,T}) \qquad (6.6)$$

for our samples.

Phenomenologically, V_T is determined by the gate voltage at which the capacitance rises out of the noise. This noise ΔC is determined by the resolution and sensitivity of the measuring technique. In the present study, ΔC varied from 0.001 to 0.03 pF depending on the ac gate-voltage amplitude, modulation frequency, etc. This produced an uncertainty of less than 0.1 V in the threshold voltage.

C. C-V turn-on characterization

The turn-on of a MOSFET capacitor is characterized not only by V_T, but also by the line shape of the C-V curve after threshold. We have chosen to characterize the line shape by the gate voltage V_{LS} corresponding to $C = \frac{1}{2}(C_{min} + C_{ox})$, an arbitrarily chosen but convenient reference point. The experimentally determined temperature, frequency, and magnetic field dependence of capacitance turn-on in a typical device are shown in Figs. 8, 9, and 10 respectively. As can be seen from these figures, V_{LS} increases with frequency and magnetic field, but varies inversely with temperature. The threshold voltage is constant within the experimental resolution of 100 mV (Fig. 10), while V_{LS} can change by as much as 1.5 V (Figs. 9, 10). An examination of the data in Fig. 10 reveals that the fine structure at turn-on occurs at voltages that are independent of magnetic field. To explain these results, the concept of bound states resulting from surface-potential variations is introduced. It is well known that point charges in the oxide and surface irregularities at the interface can profoundly affect the local surface potential.[23] The effect of such a local fluctuation would be to perturb the density of states of a 2DEG. These perturbations could behave like a localized state. We propose that such localized states are formed, and we will consider their effects.

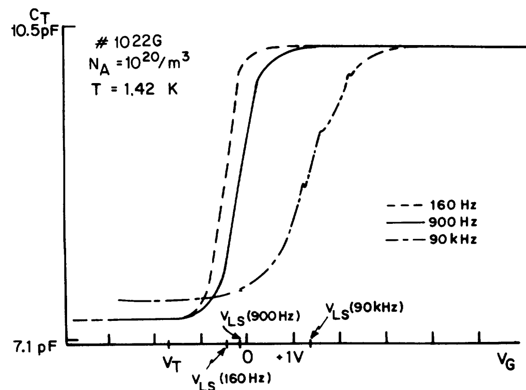

FIG. 9. Frequency dependence of the C-V curve turn-on line shape.

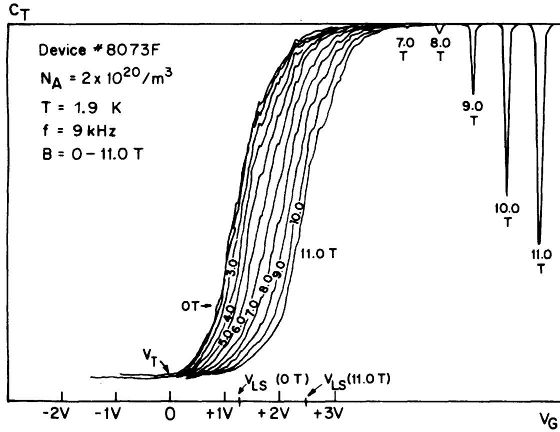

FIG. 10. Magnetic field dependence of the C_T-V_G turn-on curve. C_T is the total measured capacity.

In view of the usual numbers of oxide charges, it is important to describe these localized states and their possible properties. First of all, because of their highly localized character and relatively low concentration (presumably less than 4×10^{15} m^{-2}), they will not be subject to cyclotron motion even in the high magnetic fields employed here. As a result, we assume that these states are magnetic-field-independent. The magnetic field independence of the fine structure of Fig. 10 supports this assumption. Since the bound states are perturbed from the bottom of the 2DDS, we would expect them to overlap the conduction band (see Fig. 11) and to be distinguished from the traditional surface traps (which are generally located within the band gap) by appearing only at very low temperatures. The low-temperature requirement arises from the small binding energies of the states. Each bound state can be described in terms of a δ-function state function. It has been correctly pointed out that the bound state might be replaced or generalized to band states with a large imaginary component of the self-energy. The distribution of δ-function bound states employed in this paper is a first approximation to these nonpropagating band states. We believe our bound-state model has the added flexibility of being parametrized in terms to be discussed below. The charge in the bound states would be given by

$$Q_{BS} = -e \sum_{E_\alpha = E_1}^{E_2} \frac{\delta(E - E_\alpha)}{1+\exp[(E-E_F)/kT]}, \qquad (6.7)$$

where $\delta(E-E_\alpha)$ is the Kronecker delta at E_α (energy location of a bound state) and E_1 and E_2 are the lower and upper bounds on the energy distribution of the bound states. If the bound states are distributed in a quasicontinuous manner and are uniformly distributed in energy, Q_{BS} can be simplified to

$$Q_{BS} = -q \int_{E_1}^{E_2} \frac{N_{BS}(E)}{1+\exp[(E-E_F)/kT]} dE. \qquad (6.8)$$

N_{BS} is the density of states for the bound states. Assuming that $N_{BS}(E)$ is constant, we find that

$$Q_{BS} = (-eN_{BS}kT)\left[\frac{E_2 - E_1}{kT} + \ln\left(\frac{1+e^{u_1-u}}{1+e^{u_2-u}}\right)\right], \qquad (6.9)$$

where

$$(E_F - E_1)/kT = u - u_1,$$
$$(E_F - E_2)/kT = u - u_2,$$
$$(E_F - E_m)/kT = u = e\varphi/kT,$$

and where E_m is the intrinsic Fermi level. φ is the surface potential.

It is important to point out that when carriers in the bound states respond to the ac modulation of the surface potential, they behave as normal two-dimensional carriers. Therefore, in order to be bound states, they must have a sufficiently large relaxation time, so that carriers in them will not respond to the ac modulation frequency. However, the bound states undoubtedly have a distribution of relaxation times τ_r. The states with $\tau_r > 1/f$ will contribute to the shift in V_{LS} which depends only on dc charging of the bound states, i.e., $\Delta V_G = -\Delta Q_{BS}/C_{ox}$. If there are bound states with $\tau_r \gg 1/f$, they will not contribute to either the mobile charge or V_{LS}. In principle, the frequency dependence should provide some insight into the nonprop-

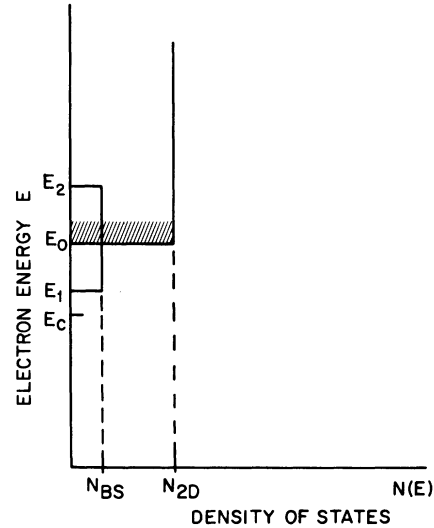

FIG. 11. Energy distribution of the bound state band $N_{BS}=A$, and the two-dimensional "heavy-mass" subband $N_{2D}=g_s g_v m_t/2\pi\hbar^2$ per unit area. The hatched region indicated that part of the 2DDS which contributes to the bound states.

agating imaginary energy states. The two-dimensional "heavy-mass" subband starts at E_0 and, when the gate voltage corresponding to $E_F = E_0$ is attained, the mobile charge contributes to the capacitance leading to

$$1/C_T = 1/C_{ox} + 1/C_{inv} . \tag{6.10}$$

The corresponding gate voltage is

$$V_G = V_T + Q_{BS}/C_{ox} + Q_{inv}/C . \tag{6.11}$$

As mentioned above, V_{LS} will be that value of V_G where $C = \frac{1}{2} C_{ox}$. To fully understand the variation of V_{LS} with temperature and magnetic field, a suitable expression for C_{inv} must be employed.

Stern[11] has obtained a self-consistent expression for C_{inv} in the electric quantum limit and the $T = 0$ K approximation. However, it is preferable to use a simpler analytic form for $C_{inv} = \partial Q_{inv}/\partial\varphi$. Using Eqs. (2.3) and (2.4), we find

$$Q_{inv} = -eN_{2D}kT[\ln(1 + e^{u-u_0})] \tag{6.12}$$

and

$$C_{inv} = e^2 N_{2D}/(1 + e^{u_0 - u}) . \tag{6.13}$$

Therefore

$$\frac{1}{C} = \frac{1}{C_{ox}} + \frac{1 + e^{u_0 - u}}{e^2 N_{2D}} , \tag{6.14}$$

but using Eqs. (6.9) and (6.13), Eq. (6.11) becomes

$$V_G = V_T + \frac{eN_{BS}kT}{C_{ox}} \left[u_2 - u_1 + \ln\left(\frac{1 + e^{u_1 - u}}{1 + e^{u_2 - u}} \right) \right] + \frac{eN_{2D}kT}{C_{ox}} \ln(1 + e^{u - u_0}) + \frac{kT}{e} (1 + e^{u_0 - u}) \ln(1 + e^{u - u_0}) . \tag{6.15}$$

From the definition of V_{LS},

$$\frac{1}{C} = \frac{2}{C_{ox}} = \frac{1}{C_{ox}} + \frac{1 + e^{u_0 - u'}}{e^2 N_{2D}} , \tag{6.16}$$

where u' is the value of u that corresponds to $V_G = V_{LS}$,

$$e^2 N_{2D}/C_{ox} - 1 = e^{u_0 - u'} , \tag{6.17}$$

and

$$V_{LS} = V_T + \frac{eN_{BS}kT}{C_{ox}} \times \left[u_2 - u_1 + \ln\left(\frac{1 + e^{u_1 - u_0}(e^2 N_{2D}/C_{ox} - 1)}{1 + e^{u_2 - u_0}(e^2 N_{2D}/C_{ox} - 1)} \right) \right] + \frac{eN_{2D}kT}{C_{ox}} \left[2 \ln\left(\frac{e^2 N_{2D}}{C_{ox}} \right) - \ln\left(\frac{e^2 N_{2D}}{C_{ox}} - 1 \right) \right] . \tag{6.18}$$

Note that $u_1 < u_0 < u_2$ so that at suitable low temperatures

$$V_{LS} \approx V_T + \frac{eN_{BS}(E_0 - E_1)}{C_{ox}} + kT \left[\frac{2eN_{2D}}{C_{ox}} \ln\left(\frac{e^2 N_{2D}}{C_{ox}} \right) - \left(\frac{N_{2D} + N_{BS}}{C_{ox}} \right) \ln\left(\frac{e^2 N_{2D}}{C_{ox}} - 1 \right) \right] . \tag{6.19}$$

Therefore, as T decreases, so should V_{LS} if N_{BS} remains constant. If N_{BS} increases with decreasing temperature, then V_{LS} will increase. Examination of Fig. 8 shows that V_{LS} increases with decreasing temperature. We can conclude that N_{BS} does increase as the temperature decreases. As we shall see later, we have other evidence corroborating this conclusion. To obtain a quantitative comparison between theory and experiment will require information on the actual 2DDS. From this, the deduction of the temperature dependence of N_{BS} should be straightforward.

As has been shown in Fig. 9, V_{LS} is also frequency dependent. From Eqs. (3.1) and (3.2), we can obtain the frequency dependence of C;

$$C = C_{ox} \frac{1 + \omega^2 R'^2 C'(C' + C_{ox})}{1 + \omega^2 R'^2 (C' + C_{ox})^2} . \tag{6.20}$$

V_{LS} is also frequency dependent through the dependence of V_G on C, i.e., from Eq. (2.3)

$$V_{LS} = V_T + \frac{Q_{BS}}{C_{ox}} + \frac{Q_{inv}^{LS}}{C_{ox}} \left(\frac{1 + \omega^2 R_{LS}'^2 (C_{LS}' + C_{ox})^2}{1 + \omega^2 R_{LS}'^2 C_{LS}'(C_{LS}' + C_{ox})} \right) . \tag{6.21}$$

As the frequency increases, V_{LS} also increases. Since Q_{inv}^{LS}, the inversion-layer charge when $V_g = V_{LS}$, should be independent of frequency and correspond to some particular value of the surface potential, the variation of V_{LS} with ω is determined by the circuit properties of the field effect device. These properties are associated with the lumped circuit parameters, R_{LS}' and C_{LS}' (the values of R' and C' at $V_g = V_{LS}$). An estimate of the importance of these quantities can be obtained by considering what happens when $\omega = 0$ and $\omega \to \infty$. From Eq. (6.21) we see that

$$(V_{LS})_{\omega=0} = V_T + \frac{Q_{BS}}{C_{ox}} + \frac{Q_{inv}^{LS}}{C_{ox}} \tag{6.22}$$

$$(V_{LS})_{\omega\to\infty} = V_T + \frac{Q_{BS}}{C_{ox}} + \frac{Q_{inv}^{LS}}{C_{ox}} + \frac{Q_{inv}^{LS}}{C_{LS}'} = (V_{LS})_{\omega=0} + \frac{Q_{inv}^{LS}}{C_{LS}'} . \tag{6.23}$$

In view of the fact that the MOSFET is a distributed element, the lumped element C_{LS}' will be frequency dependent. Hence the frequency correction may be quite substantial, and V_{LS} is shifted to move positive values, as found experimentally.

If the experimental frequency is such that a strong interdependence of surface resistance and surface capacitance does not exist, then the magnitude of the capacitance dips will be frequency inde-

pendent. However, once the frequency becomes appreciable, the magnitude of the dips becomes larger, and will be frequency dependent (see Fig. 15). Consequently, in order that these capacitance dips be within 5% of their actual value in devices of the type employed, the experimental frequency must be less than 900 Hz.

The magnetic field dependence of V_{LS} (see Fig. 10) can also be accounted for in terms of the bound-state band in Fig. 11. Because of the magnetic field, the 2DDS of Fig. 11 must be redistributed into Landau levels starting at $E_0 + \frac{1}{2}\hbar\omega_c - sg\mu_B B$. This can be written formally as

$$N_{2D} = \hbar\omega_c N_{2D} \sum_{n,s,v} \delta(E - E'(n, s, v)), \qquad (6.24)$$

where E' is defined by Eq. (2.6). The charge associated with these states is

$$Q_{inv} = -e\hbar\omega_c N_{2D} \sum_{n,s,v} (1 + e^{u'-u})^{-1}, \qquad (6.25)$$

where $u' = E'/kT$. Setting $n = 0$, $v = 0$, and $s = -\frac{1}{2}$, the gate voltage in the vicinity of turn-on is, for the first Landau level,

$$V_G = V_T + \frac{eN_{BS}kT}{C_{ox}}\left[\frac{E_2 - E_1}{kT} + \ln\left(\frac{1 + e^{u_1 - u}}{1 + e^{u_2 - u}}\right)\right] + \frac{e\hbar\omega_c N_{2D}/C_{ox}}{1 + \exp(u_0 - u + \xi\hbar\omega_c/kT)} + \frac{kT}{e}\left[1 + \exp(u - u_0 + \xi\hbar\omega_c/kT)\right], \qquad (6.26)$$

and the capacity is

$$\frac{1}{C} = \frac{1}{C_{ox}} + \frac{kT}{e^2 N_{2D}\hbar\omega_c}(1 + e^{u - u_0 - \xi\hbar\omega_c kT})(1 + e^{u_0 + \xi\hbar\omega_c kT - u}). \qquad (6.27)$$

Here too, we wish to use the condition for V_{LS}, i.e., $C = \frac{1}{2}C_{ox}$. If we let $e^2 N_{2D}\hbar\omega_c/C_{ox}kT \gg 1$, then V_{LS} can be written as

$$V_{LS} \approx V_T + (E_0 - E_1 + \xi\hbar\omega_c)eN_{BS}/C_{ox} + 2kT/e. \qquad (6.28)$$

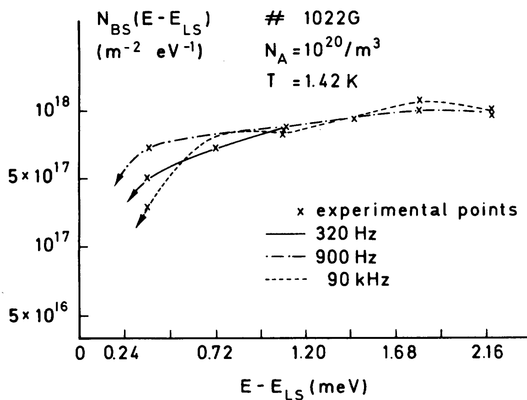

FIG. 12. Frequency dependence of the bound-state density of states measured relative to E_{LS}.

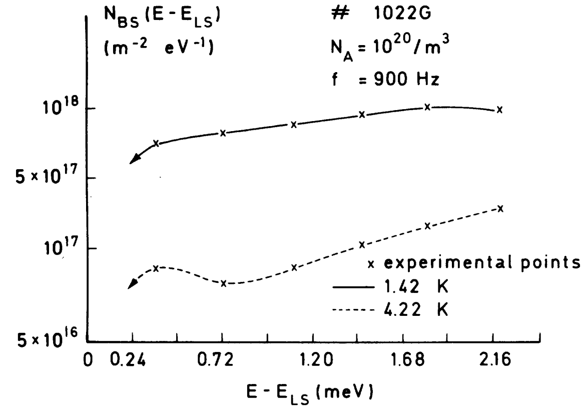

FIG. 13. Temperature dependence of the bound-state density of states measured relative to E_{LS}.

If we recall that the data in Fig. 10 indicates a uniformly spaced *shift* in V_{LS} with increasing magnetic field, then

$$\Delta V_{LS} = (eN_{BS}/C_{ox})\Delta\xi\hbar\omega_c. \qquad (6.29)$$

In other words, the zero-point energy shift of $\xi\hbar\omega_c$ is "uncovering" more bound states which must be charged by V_G as the magnetic field is increased. Therefore, the change in V_{LS} with magnetic field is correlated to the total number of states uncovered by the $\xi\hbar\omega_c$ shift. This can be written as

$$\Delta V_{LS} = -\Delta Q_{BS}/C_{ox} = -(-q\Delta n_{BS})/C_{ox}), \qquad (6.30)$$

where Δn_{BS} is the increase in the number of uncovered bound states. The density of states can now be calculated by

$$N_{BS} = \Delta n_{BS}/\Delta\xi\hbar\omega_c. \qquad (6.31)$$

Although Eq. (6.31) gives the density of bound states, the energy location of the Fermi level within the conduction band corresponding to V_{LS} at $B = 0$, i.e., E_{LS}, is not known. Therefore, we can obtain information about N_{BS} relative to E_{LS}, but do not know the relationship between E_{LS} and E_0. To indicate this, N_{BS} is replaced by $N_{BS}(E - E_{LS})$. In Figs. 12 and 13 the frequency and temperature dependence of $N_{BS}(E - E_{LS})$ are shown.

For the sample of Figs. 12 and 13, the number of interface charges at room temperature was $+3.84\times10^{15}/m^2$. These oxide charges have been attributed to alkali ions.[18] In Fig. 18, data is presented for the gate-voltage dependence of the capacity as a function of magnetic fields. Examination of this data shows a marked difference between the amount of charge in the first spin-split level and the higher levels. Other data fully confirm the fact that the first spin-split level contains less charge than do the subsequent levels. Fang, Fow-

ler, Howard, and Stiles[2] made similar observations on conductance, though the precision of the conductance measurement in this region of gate voltages is significantly less than that of the capacitance measurement. The capacitance data indicates that 1.4×10^{15} charges/m^2 are "missing" from the first spin-split $n=0$ level. If the bound-state model we are employing is valid, we would expect that no more than 1.4×10^{15} states/m^2 will be uncovered as the magnetic field increases. The bound state density Δn_{BS} from Eq. (6.31) is $1.0\times10^{15}/\mathrm{m}^2$ for $B=12$ T. This is encouraging and consistent. It also implies that there are $0.4\times10^{15}/\mathrm{m}^2$ states still available at higher energies (i.e., for $B>12$ T). Indeed, if the bound-state density is constant up to its cut-off, as suggested in Fig. 11, then the cut-off field for seeing all of these states would be 17 T.

The data in Fig. 12 indicates a negligible variation in N_{BS} with frequency, though the data in Fig. 9 indicates a strong dependence of V_{LS} on frequency. We can readily explain this difference with Eq. (6.23). The change in V_{LS} due to frequency is associated with the inversion-layer mobile charge. Application of a magnetic field, as indicated in Eqs. (6.26) and (6.28), will influence the point where mobile charge becomes important, but that should not influence the frequency dependence of any parameters. Hence, Q_{inv}^{LS} will be the same for both zero and large magnetic fields, in both low- and high-frequency cases. Hence, the change in V_{LS} with field will be frequency independent until N_{BS} becomes frequency dependent at very low frequencies. As mentioned earlier, the frequency dependence of the bound states should relate to possible continuum states with imaginary self-energies.

As indicated by the discussion of Eq. (6.19), N_{BS} can be temperature dependent, and this is clearly seen in Fig. 13. The use of the magnetic field dependence of V_{LS} to uncover the form of N_{BS} is an important result of this work. Recently, Pals investigated the effect of x-ray-induced additional interface charges.[24] He concluded that the motion perpendicular to the surface is broadened by the interface charge. Without introducing a bound-state density, his results can be viewed as being suggestive of its existence. Additional measurements are needed to confirm the role of additional charges in the oxide on N_{BS}.

To recapitulate, it has been shown that a bound-state band located at the conduction-band edge influences both the line shape of C near threshold and V_{LS}. The bound-state band can be investigated by means of the magnetic quantization of the two-dimensional mobile charge.

D. Magnitude of capacitance minima

As can be seen from Fig. 14, the magnitude of the capacitance dips increases with increasing magnetic field and decreasing temperature. This is reasonable because an increasing magnetic field increases the quantum level separations, thereby lowering the density of states at the minimum point. Also, decreasing temperature causes a narrowing of the Fermi surface, which will also sharpen the capacitance dips.

It was found that the capacitance dips disappear if the surface potential is overmodulated by the ac gate voltage, a point that has been poorly understood in the past.[10] This is due to the fact that, for a given surface electric field modulation, the band-bending excursion will increase when the Fermi level is at a minimum density-of-states condition. Consequently, the Fermi-level excursion can be from the tail of one quantum level to the beginning of the next quantum level. Since it is the average over this excursion that is measured experimentally, it is possible to measure a higher effective density of states than the true minimum value.

In their original work, Kaplit and Zemel[3] employed a δ-function model as a first-order approximation to describe the Landau levels. It was noted that some broadening was needed to account for the voltage dependence of the capacitance minima. Ohta has conducted a far more detailed theoretical investigation of broadening of the Landau levels

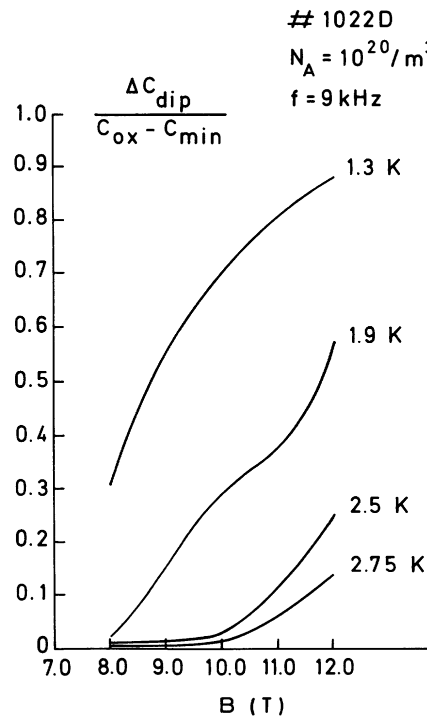

FIG. 14. Temperature dependence of the normalized capacitance minimum for the spin-split $n=0$ Landau level.

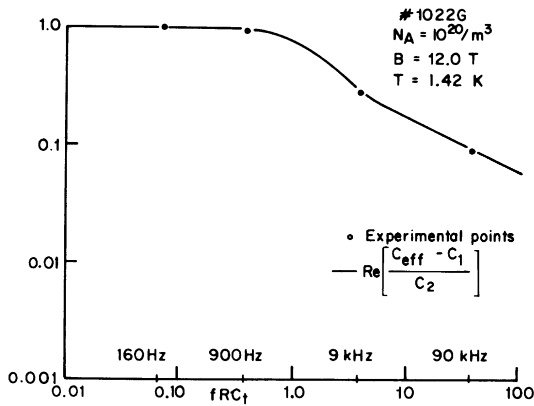

FIG. 15. Frequency dependence of the $n = 0$ spin-split capacitance minimum.

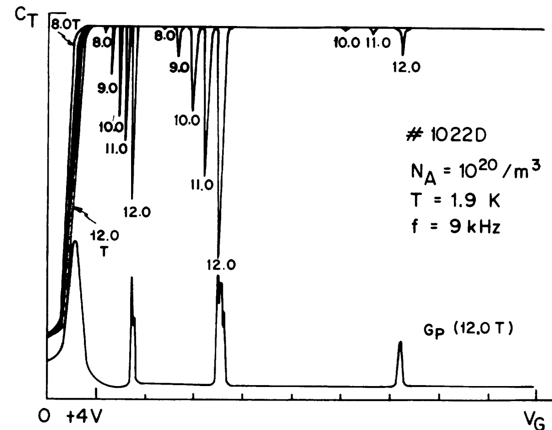

FIG. 17. C-V curves for $B = 80$, 90, 100, 110, and 120 T, and the G_p-V curve for $B = 120$ T. The $n = 0$ spin-split Landau level and the $n = 1$ Landau level can be seen from the C-V curves.

observed by both admittance[12] and transconductance.[13] As a result, he concludes that an impurity-type scattering is essential for describing the gate-voltage dependence of the capacitance minima. The general features of the capacitance dips measured here agree with the earlier measurements. The capacitance minima is largest between the Landau levels. Spin-splitting is resolved at higher magnetic fields, and only at the highest magnetic fields and lowest temperatures can valley splitting be resolved. If there was no broadening of the magnetic quantum levels, then the C-V curve would occur as shown in Fig. 16 and as pointed out by Ohta.[12] Since dips (rather than the abrupt drop) in capacitance of Fig. 16 are observed experimentally, this indicates that broadening of the quantum levels cannot be neglected.

E. Equivalent parallel conductance (G_p) phenomena

Since G_p is dependent on C' and R' (Sec. III A), it is found that G_p reflects much of the same phenomena as C and g'_{SD}. For instance, as V_{LS} increases with magnetic field, there is a similar shift in the G_p peak associated with turn-on. At the minimum density of states between Landau levels where C exhibits minima, G_p exhibits maxima as discussed earlier. However, the maxima observed show a splitting (see Fig. 18). It can be shown that this occurs because of the different V_G dependence of R' and C'. A detailed study of G_p indicates that as many as two maxima are easily possible. However, multiple splittings are observed (see second Landau peak in Fig. 17) and no explanation based on simple lumped circuit arguments seems to account for this behavior. Because spin and valley splittings are not as large as the Landau separations, the G_p maxima for these quantum levels will not be as large as for the Landau separations, and the relative minima observed in the G_p peaks are not as pronounced either. This is, of course, due to the fact that the variation of R' and C' will not be as large for these levels as for Landau separations.

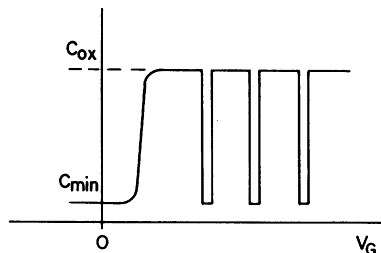

FIG. 16. Ideal C-V curve for the case of negligible Landau-level broadening at a constant magnetic field.

F. Source-drain surface conductance (g_{SD}) phenomena

The source-drain conductance experiments yielded the same structure as has been previously reported.[2] In this study, surface conductance was performed along with C-V experiments for comparative purposes. It was found that g_{SD} is so small at V_T that it could not be observed. Instead, the onset of appreciable conductance occurs at a pseudothreshold voltage which does not correspond to either the bound-state threshold or the inversion-layer mobile carrier threshold as seen in Fig. 18. Usually, the g_{SD} pseudothreshold is from 4 to 6 V greater than V_T or V_{LS} found in capacitance studies on the same devices. We conclude that surface conductance experiments lack the sensitivity and resolution necessary to study turn-on behavior near V_T and V_{LS}.

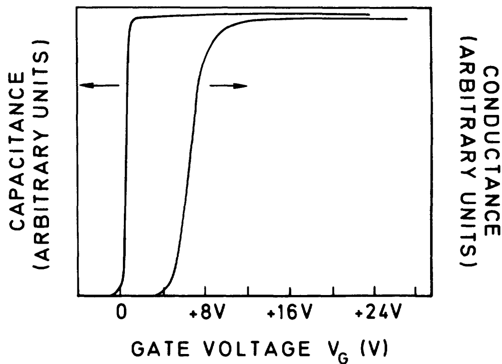

FIG. 18. Comparison of C-V vs G-V plots for sample No. 1022H at $B=0$ and $T=1.42$ K. Note the substantial difference between the turn-on voltages for capacitance and conductance (~4 V).

VII. CONCLUSIONS

The current study has shown the usefulness of surface admittance as an experimental tool in investigating surface-quantization phenomena. In addition, the comparative study of both surface admittance and conductance has established the interrelationship and useful regimes of both techniques. The existence of bound-state behavior resulting from the perturbation of the two-dimensional mobile charge subband by oxide charges is proposed. These bound states arise at the bottom of the 2DDS and influence the characteristics of the admittance near threshold. Therefore, surface admittance should be sensitive to the distribution of the oxide charge normal to the interface, as well as to the magnitude of the oxide charge. The magnetoadmittance measurements sensitivity to perturbations of the surface potential should be of substantial use in the evaluation of the effects of fixed oxide and surface charge, surface roughness, and other physical and chemical imperfections on semiconductor surfaces. It is felt that the advantages of high resolution and sensitivity of magnetoadmittance measurements, plus their nondestructive nature, make this technique a viable tool in the investigation of properties of surface-quantized semiconductors, despite the necessity of high magnetic fields and cryogenic temperatures. The two-dimensional character of the electron gas associated with a highly inverted surface has been further substantiated.

ACKNOWLEDGMENTS

The authors would like to express their appreciation to Dr. A. B. Fowler and the IBM Research Laboratories for their assistance in providing specimens for this research. They would also like to thank F. F. Fang, A. B. Fowler, F. Stern, P. J. Stiles and R. F. Greene for many useful discussions of surface-quantization phenomena.

---

*This work was supported by an Advanced Research Projects Agency Contract (0251) to the Laboratory for Research on the Structure of Matter.

†Present address: Bell Telephone Laboratory, Murray Hill, New Jersey.

[1]J. R. Schrieffer, in *Semiconductor Surface Physics*, edited by R. H. Kingston (University of Pennsylvania, Philadelphia, 1957), p. 68.

[2]F. F. Fang, A. B. Fowler, W. E. Howard, and P. J. Stiles, Phys. Rev. Lett. 16, 901 (1966).

[3]M. Kaplit and J. N. Zemel, Phys. Rev. Lett. 21, 212 (1968).

[4]F. F. Fang and D. J. Stiles, Phys. Rev. 174, 823 (1968).

[5]C. B. Duke, Phys. Rev. 159, 632 (1967).

[6]C. B. Duke, Phys. Rev. 168, 816 (1967).

[7]R. W. Ralston, Ph.D. thesis (Yale University, 1971) (unpublished).

[8]R. W. Ralston and R. G. Wheeler, Phys. Rev. Lett. 27, 925 (1971).

[9]F. Stern and W. E. Howard, Phys. Rev. 163, 816 (1967).

[10]F. Stern, in *Proceedings of the Tenth International Conference on the Physics of Semiconductors* (U. S. AEC, Oak Ridge, Tenn., 1970), p. 451.

[11]F. Stern, Phys. Rev. B 5, 4891 (1972).

[12]K. Ohta, Jap. J. Appl. Phys. 10, 850 (1971).

[13]K. Ohta, J. Phys. Soc. Jap. 31, 1627 (1971).

[14]Tsuneya Ando (private communication).

[15]Y. Matsumoto (private communication).

[16]H. Ezawa, S. Kawaji and K. Nakamura, Surf. Sci. 27, 218 (1971).

[17]D. K. Wilson and G. Feher, Phys. Rev. 124, 1068 (1961).

[18]A. S. Grove, *Physics and Technology of Semiconductor Devices*, (Wiley, New York, 1967), Chap. 3.

[19]The magnetic field was produced by a Bitter magnet in the High Field Magnet Laboratory of the University of Pennsylvania.

[20]A. Goetzberger, Bell Syst. Tech. J. 45, 1097 (1966).

[21]F. P. Heiman and H. S. Miller, IEEE Trans. Electron Devices 12, 142 (1965).

[22]B. E. Deal, M. Sklar, A. S. Grove, and E. H. Snow, J. Electrochem. Soc. 114, 266 (1967).

[23]R. F. Greene, *Molecular Processes on Solid Surfaces*, edited by E. Drauglis, R. D. Gretz and R. I. Jaffee (McGraw-Hill, New York, 1969), p. 239.

•[24]J. A. Pals, Phys. Rev. B 7, 754 (1973).